Kluge, C., Milsch, H., Blöcher, G. (2017): Permeability of displaced fractures. - *Energy Procedia*, *125*, pp. 88—97.

DOI: http://doi.org/10.1016/j.egypro.2017.08.077

Available online at www.sciencedirect.com

ScienceDirect

Energy Procedia 125 (2017) 88–97

Energy Procedia

www.elsevier.com/locate/procedia

European Geosciences Union General Assembly 2017, EGU Division Energy, Resources & Environment, ERE

Permeability of displaced fractures

Christian Kluge[a,*], Harald Milsch[a], Guido Blöcher[a]

[a]*Helmholtz Centre Potsdam GFZ German Research Centre for Geosciences, Telegrafenberg, 14473 Potsdam, Germany*

Abstract

Flow along fractures becomes increasingly important in the context of geo-engineering applications. Commonly, the permeability of fractures is approximated using the cubic law assumption. However, fracture flow is influenced by the surface roughness and the relative shear displacement. A numerical approach was used which calculates the flow pattern within a rough fracture. Therefore, fracture surfaces are generated using a power spectral density function and fracture flow is simulated under the incompressible Navier Stokes approximation. It is shown that the cubic law solution overestimates the permeability as modeled by the 3D numerical simulation of flow in fractures.

Peer-review under responsibility of the scientific committee of the European Geosciences Union (EGU) General Assembly 2017 – Division Energy, Resources and the Environment (ERE).

Keywords: fracture permeability; flow in fractures; fracture roughness; cubic law

1. Introduction

Flow along fractures or in fissured systems becomes increasingly important in the context of Enhanced Geothermal Systems (EGS), shale gas recovery or nuclear waste disposal. Fault zones and natural fracture networks are more and more considered as main reservoir targets, for example the geothermal exploitation in the Southern German Molasse Basin [1]. An approximation of the potential of fracture transmissivity is therefore an important topic. In reservoir simulations, commonly, a constant fracture aperture is used to describe permeability in a fracture or in fracture networks. The permeability of fractures is approximated using the Hagen-Poiseuille solution of the Navier Stokes equation. Flow in fractures is assumed to be laminar between two parallel plates separated by a constant distance a, such that the fracture permeability k_f can be derived from the cubic law approximation [2]:

$$k_{f,cubic} = \frac{a^2}{12} \tag{1}$$

* Corresponding author. Tel.: +49-30-288-27527 ; fax: +49-30-288-1577.
E-mail address: christian.kluge@gfz-potsdam.de

1876-6102
Peer-review under responsibility of the scientific committee of the European Geosciences Union (EGU) General Assembly 2017 – Division Energy, Resources and the Environment (ERE).
10.1016/j.egypro.2017.08.077

However, it is a well-known fact, that fracture flow is strongly influenced by the fracture surface roughness and the shear displacement along the fracture planes [3, 4, 5]. Furthermore, the orientation of the pressure gradient in respect to the aperture field is causing a strong variability of the hydraulic behaviour of a rough fracture [6]. Correction factors for the aperture to calculate the cubic law permeability were therefore introduced by several authors. Méheust and Schmittbuhl [7] studied the deviation of the cubic law for a natural fracture surface and plexiglas, observing higher deviations from the cubic law for small apertures, which are correlating to the same trend in experimental investigations. Zimmerman & Bodvarsson [3] corrected the aperture a, considering the mean aperture, ⟨a⟩, a surface roughness factor, C_r, and a tortuosity factor, C_t, that was later modified by Walsh et al. [4]:

$$a = \langle a \rangle \cdot C_r \cdot C_t \tag{2}$$

Jin et al. [5] introduced a semi-empirical function using fitted parameters depending on the surface geometry accounting for the surface roughness, as well as for the hydraulic and surface tortuosity effect. We are providing a fracture flow simulation considering 3D Navier Stokes flow for rough and displaced fractures. We further provide a quantification of the deviation from the cubic law permeability. The controlling parameters on fracture permeability of rough and displaced fractures are discussed.

2. Methods

The workflow for the fracture flow simulation in a 3D fracture comprises three main steps: (1) generating fracture topographic surfaces with varying roughness and displacement, (2) generating a finite element mesh to produce a 3D model of a fracture, (3) perform fracture flow simulations using Navier Stokes flow in the finite element software Comsol Multiphysics (www.comsol.de), to derive fracture permeability from the pressure and velocity field using Darcy's law.

2.1. Fracture topography generation

Rock fracture surface anisotropy can be captured by power spectral density formulations [8]. The following simplified equations were used to generate fracture topographies following a power law with a uniform random signal:

$$h = P_0^{0.5} \cdot \frac{h_0}{S} \tag{3}$$

$$S = i(x, y)^{B/2} \tag{4}$$

where h is the asperity height, P_0 the multiplier amplitude, h_0 is the normalised random height distribution i the location of a point and B the amplitude scaling factor influencing the roughness. A small B value produces rough fractures, whereas large B values produce smooth fracture topographies. The power $B/2$ is used because the power spectral density is proportional to the amplitude squared. The fracture aperture distribution is a normalized Gaussian distribution as it is commonly observed for natural fracture surfaces. The script allows to produce fracture surfaces of 100x100 mm or any other quadratic size.

Assuming that tensile fracturing will naturally produce two fracture surfaces that are perfectly matching and equal in shape, two equal surfaces are generated and super-positioned based on their minimum contacting points. The aperture is calculated as the subtraction of the upper and the lower asperity height at each point. When both fracture surfaces have no displacement relative to each other, the overall aperture is zero, since both fracture are perfectly matching. To implement a shear displacement, the top surface is displaced relative to the bottom surface by shifting the spatial point cloud data by a 1 mm increment in the y-direction to a maximum displacement of 50 mm. Every point that has no spatial correlation on the bottom surface is again added to the opposite side of the fracture using the "circshift" function in Matlab (fig. 1a). This means that by displacing the upper fracture surface by 100 mm, both surfaces are again matching. The distance between the two surfaces, i.e. the aperture, is recalculated at every step based on the minimum contacting points. Therefore, each change in displacement leads to a change in mean aperture (fig. 1b). The advantage of this approach is that the length of the fracture stays constant. However, this approach excludes any mechanical deformation of the fracture asperities, i.e. fracture asperities have an infinite stiffness. The

fracture apertures in our models are in the range of a few 0.5 to 2.5 mm in our study, which describe a lower bound of the real spectra. Hydraulic apertures filled with proppants in reservoirs range from 0.2 mm to 2 cm [9, 10]. On laboratory scale, however, fracture apertures are some μm and therefore not comparable to our results [11, 12].

The spatial point cloud data is then exported to the software "MeshIt" [13]. MeshIt allows to create a 3D finite element mesh based on spatial point cloud data. The fracture topographic surface is interpolated using the Inverse Distance Weighting method (IDW). The mesh was refined at the inflow and outflow boundaries to allow for a more precise calculation of the pressure field. The element size of the respective fracture models was around 150000-300000 elements.

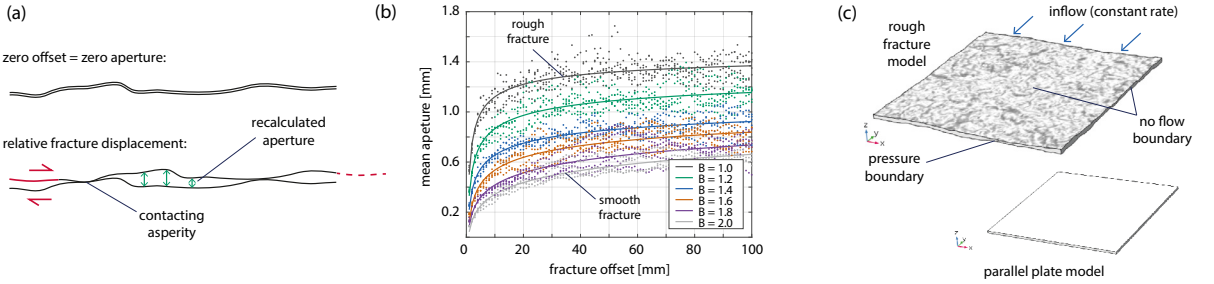

Fig. 1. (a) Illustration of the applied method to create a shear displacement between two equal fracture topographic surfaces. (b) The mean aperture increases strongly at low fracture offset, but is changing less after around 15 mm of fracture displacement, i.e. when the elevations of the initially neighbouring asperities are overcome. (c) 3D model of a rough fracture with constant flow applied at the inlet and a pressure boundary at the outlet, as well as the parallel plate model for the verification of results.

2.2. Fluid flow simulations

Comsol Multiphysics (www.comsol.de) allows to simulate the flow in saturated void space using the free flow physics tool, which is based on the Navier Stokes approximation using the continuum equation for incompressible flow (with $\nabla \cdot u = 0$):

$$\underbrace{\rho\left(\frac{\partial u}{\partial t} + u \cdot \nabla u\right)}_{\text{inertial forces}} = \underbrace{-\nabla p}_{\text{pressure forces}} + \underbrace{\nabla \cdot (\mu(\nabla u + (\nabla u)^T) - \frac{2}{3}\mu(\nabla \cdot u)I)}_{\text{viscous forces}} + \underbrace{F}_{\text{external forces}} \tag{5}$$

where u is the fluid velocity, p is the fluid pressure, ρ is the fluid density, μ is the fluid dynamic viscosity, I is the identity matrix and F are the external forces. The first term describes the inertial forces, which is assumed to be negligible in our models, the second term the pressure forces, the third term the viscous forces and F the external forces applied to the fluid, i.e. gravity. However, gravity has almost no impact for the apertures of a few millimeters. The 3D finite element mesh was imported to Comsol and the following boundary conditions were applied to the model: (1) constant flow rate at the inlet, (2) zero bar pressure boundary at the outlet (relative to atmospheric pressure) and (3) no flow (no slip) condition at the boundaries (fig. 1c). The parameters used for the simulation are a constant inflow velocity v or u of 1e-3, 1e-4 and 1e-5 m/s, as well as a temperature dependent fluid density ρ and dynamic fluid viscosity μ (constant room temperature). Flow was imposed parallel to the displacement direction of the fracture along the y-axis. The simulation is a time dependent, transient solution, calculating results every 60 sec up to a total simulation time of 3600 sec. A steady state pressure regime was observed within the first 60 sec in all simulations. The permeability of the fracture was calculated using Darcy's law for laminar flow. The pressure gradient was calculated using the mean inflow and outflow pressure at the boundaries. Three different inflow velocities were chosen such that laminar flow conditions are met ($Re < 1400$) by calculating the Reynolds number for two parallel plates:

$$Re = \frac{av\rho}{\mu} \tag{6}$$

where a is the aperture at each point of the fracture, v the flow velocity at each point of the fracture, ρ the fluid density (constant) and μ the fluid viscosity (constant). The aperture distribution $a(x, y)$ was taken from the generated

fracture topography model and the velocity $v(x, y)$ was exported from the Comsol simulation. Interpolation of the x and y coordinates of the velocity field to those of the aperture field gives a spatial model for the Reynolds number using equation 6. Two examples for a spatial distribution of the Reynolds number are shown in figure 2. Although increasing the inflow velocity and therefore the Reynolds number led to numerical instability of the simulations, the Reynolds number never exceeded conditions for laminar flow ($Re < 1400$). Five models at five different displacement levels ($d = 1$ mm, $d = 5$ mm, $d = 10$ mm, $d = 25$ mm and $d = 50$ mm) were used for the simulation. Furthermore, three different roughness levels were used ($B = 1$, $B = 1.5$, $B = 2$). A total of 45 flow simulations have been performed. However, not all simulations were successful due to numerical instability for certain cases.

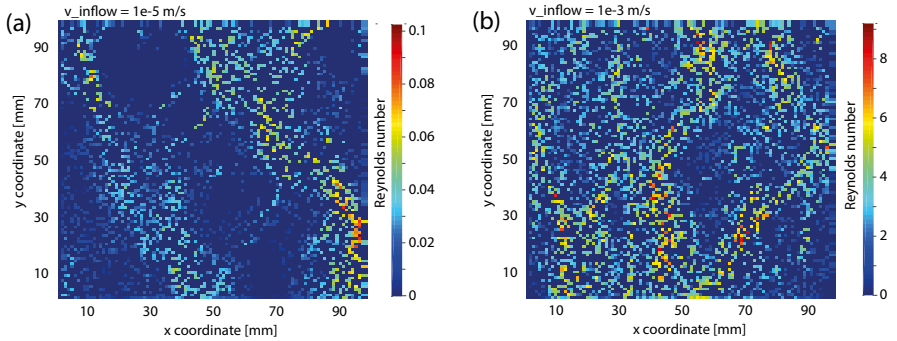

Fig. 2. Spatial distribution of the Reynolds number for (a) 50mm displacement, medium roughness (B = 1.5), inflow velocity 1e-5 m/s and (b) 50mm displacement, high roughness (B = 1), inflow velocity 1e-3 m/s. The maximum Reynolds number is less than 10, such that flow is laminar in all simulations.

2.3. Model verification

To verify the results from the numerical simulations, flow through two parallel plates, separated by a constant distance of $a = 1.5$ mm, representing about the average aperture of all simulations, was simulated. The same boundary conditions as for the rough fractures were used. Comparing the results of flow through two parallel plates in a 3D simulation and the analytical solution given by the cubic law (eq. 1), the simulation provides an accuracy within 1% (see table 1).

3. Results

The simulations were evaluated in terms of the dependence of fracture permeability on fracture roughness and displacement. The fluid pressure distribution and velocity field is used to demonstrate the change in flow pattern from the 3D flow simulations. The permeabilities obtained from the simulations were compared to the fracture permeability calculated from the cubic law approximation (eq. 1). The results are summarized in table 1. The maximum Reynolds number *Re* is given for the inflow velocity of 1e-4 m/s (range of *Re* is always between 0 and Re_{max}).

Table 1. Parameters and results for simulations at various displacement and for fractures of different roughness.

d (*mm*)	B (-)	Re_{max} (-)	$\langle$ a $\rangle$ (*mm*)	$k_{f,cubic}$ (m^2)	$k_{f,numerical}$ (m^2)	$k_{f,numerical}$ / $k_{f,cubic}$
5	1.0	0.83	1.7891	$2.6673e^{-7}$	$8.4717e^{-8}$	0.32
	1.5	0.51	0.9745	$7.9145e^{-8}$	$1.7234e^{-8}$	0.22
	2.0	0.15	0.5529	$2.5474e^{-8}$	$5.5658e^{-9}$	0.22
10	1.0	0.85	1.8352	$2.8065e^{-7}$	$1.0792e^{-7}$	0.38
	1.5	0.89	1.2202	$1.2408e^{-7}$	$2.9994e^{-8}$	0.24
	2.0	0.89	0.7353	$4.5055e^{-8}$	-	-
25	1.0	0.78	2.0580	$3.5294e^{-7}$	$1.5763e^{-7}$	0.45
	1.5	0.99	1.5723	$2.0600e^{-7}$	$7.6535e^{-8}$	0.37
	2.0	0.57	1.0769	$9.6650e^{-7}$	$1.7279e^{-8}$	0.18
50	1.0	0.91	2.3776	$4.7109e^{-7}$	$2.1839e^{-7}$	0.46
	1.5	1.03	1.6832	$2.3609e^{-7}$	$1.1027e^{-7}$	0.47
	2.0	0.95	1.1563	$1.1142e^{-7}$	$2.3940e^{-8}$	0.21
parallel plates	-	0.15	1.5000	$1.8750e^{-7}$	$1.8744e^{-7}$	0.99

3.1. Aperture distribution

The aperture distribution across one fracture is a normal Gaussain distribution by definition of the power spectral density function used for the fracture surface generation. However, the range of aperture distribution is changing with the relative fracture displacement. Generally, the higher the fracture displacement the higher the mean aperture (fig. 1) and the wider the range or distribution of the aperture (fig. 3). This behaviour is different for different fracture roughnesses, but the trend is similar in all cases. After a certain threshold in displacement, i.e. d = 15 mm in our simulations, the mean aperture magnitude and the distribution are not changing significantly anymore. The magnitude of the aperture is dependent on fracture roughness. Rough fractures have a higher mean aperture than smooth fractures when being displaced.

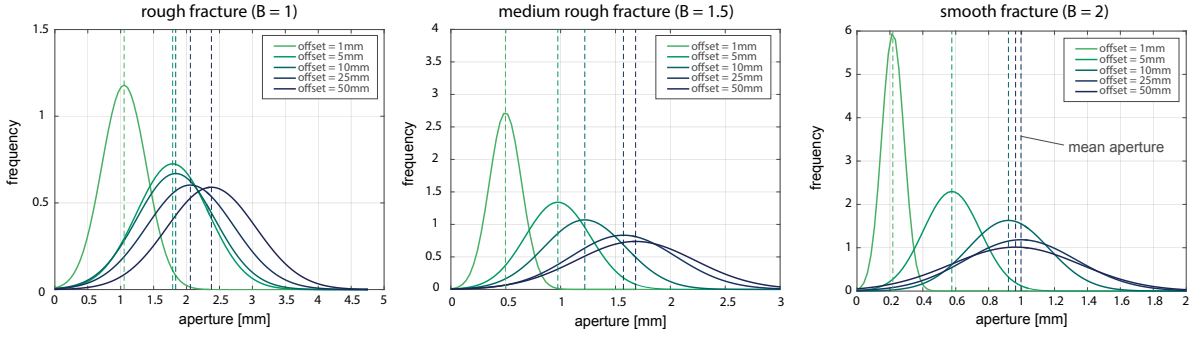

Fig. 3. Probability density function of aperture distribution for different fracture offsets showing and increase in mean aperture and an increase in aperture range for increasing offsets.

3.2. Increasing fracture displacement

The flow velocity magnitude field allows to describe the flow pattern within a rough fracture. The velocity and pressure distribution of a fracture with constant roughness ($B = 1.5$) and increasing displacement was analysed. Figure 4 shows a cut through the middle of the fracture plane, displaying pressure and fluid velocity. For small displacements small flow channels with low velocities were simulated. With increasing displacement, channels become wider and are getting connected having higher flow velocities. At a displacement of $d = 25$ mm the flow field already covers large areas of the fracture. The pressure gradient is very small in all simulations. The reason for that is the large aperture and therefore the high hydraulic permeability. However, higher inflow velocities led to some numerical instability. Calculating the fracture permeability from the simulation data, permeability follows the same general trend as the aperture with increasing displacement, i.e. the more displaced a fracture the higher its permeability.

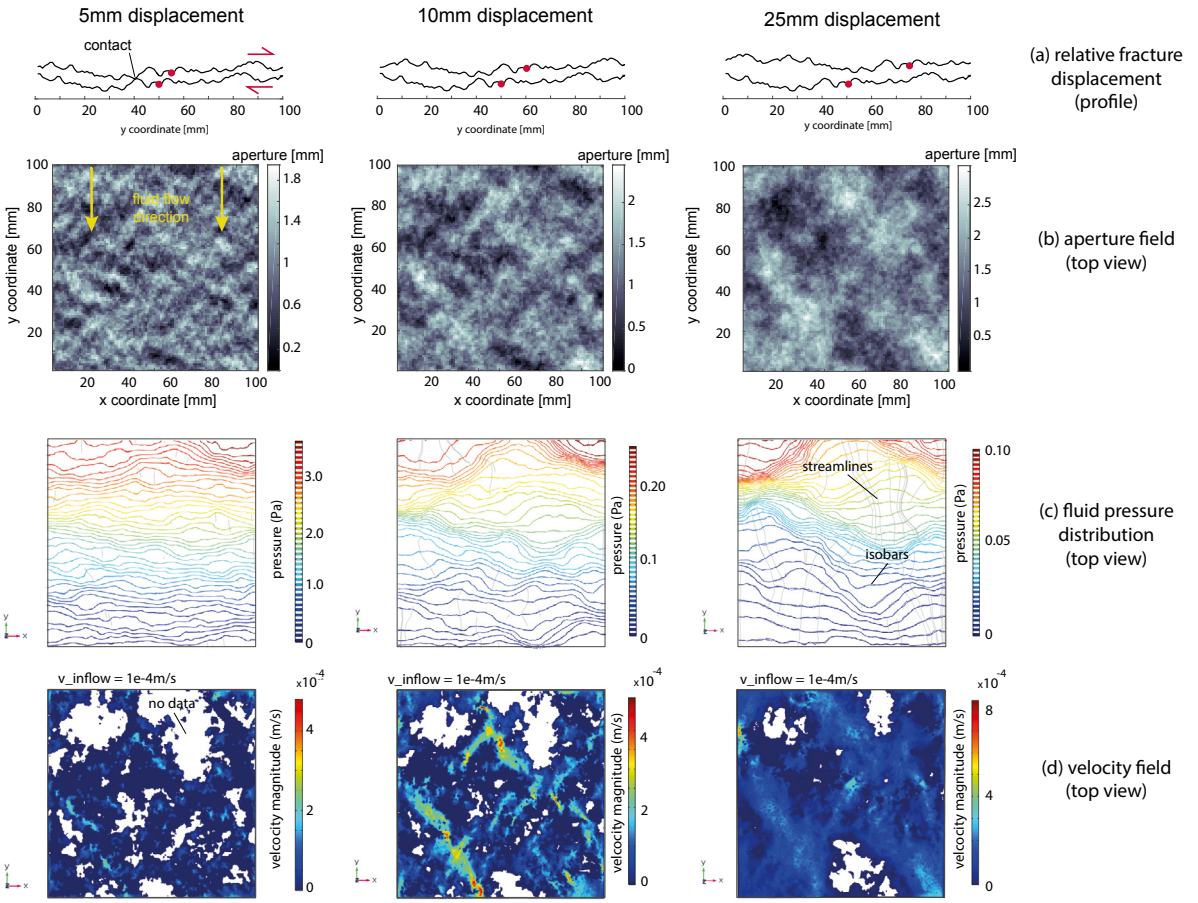

Fig. 4. (a) Fracture aperture profiles showing a profile of the displaced fracture, (b) aperture distribution across the fracture, (c) fluid pressure distribution (zero pressure = atmospheric pressure) with stream lines and (d) velocity magnitude field across the fracture. The roughness is constant with $B = 1.5$ for all fracture models, whereas displacement was varied. Generally, the flow velocity is zero or close to zero in areas of low aperture. The distribution of low and high aperture regions depends on the displacement. Higher displacement causes continuous flow with higher velocity distributed all over the fracture void space. Less displaced fractures, in contrast, show very localised flow with small channels and discontinuous streamlines.

3.3. Increasing fracture roughness

The dependence of fracture roughness on the flow behaviour was analysed, as well. For these simulations, the displacement of all fractures was set to 50mm and roughness levels of $B = 1$, $B = 1.5$ and $B = 2$ were used. Figure 5 shows a cut through the middle of the fracture plane, displaying pressure and fluid velocity. For rough fractures, large and continuous channels are distributed over the entire area of the fracture void space. Smooth fractures, in contrast, show very localised flow since aperture in some local areas is either high, or close to zero. The evaluation shows that the effective fracture permeability is only between 20% and 50% of the analytical solution without corrections (fig. 6). Rough fractures show a systematic decrease in deviation with increasing fracture offset, whereas smooth fractures show no clear trend. The permeability is generally lower for smooth and displaced fractures compared to rough and displaced fractures.

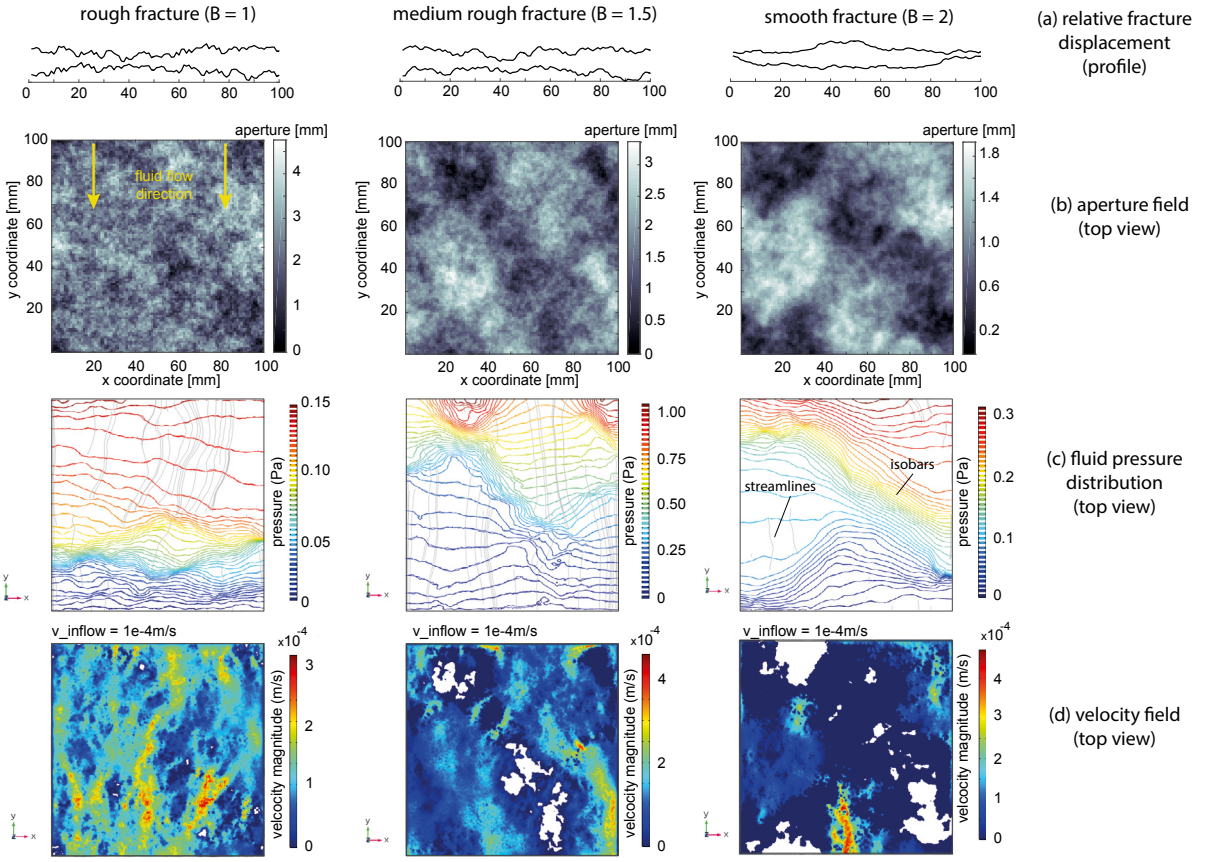

Fig. 5. (a) Fracture aperture profiles showing a profile of the the fractures with different roughness, (b) aperture distribution across the fracture, (c) fluid pressure distribution (zero pressure = atmospheric pressure) with stream lines and (d) velocity magnitude field across the fracture. The displacement d is constant at 50 mm for all fracture models, whereas roughness was varied. Generally, the flow velocity is zero or close to zero in areas of low aperture. The distribution of low and high aperture regions depends on the roughness. Higher roughness causes continuous flow with higher velocity distributed all over the fracture void space. Smooth fractures, in contrast, show very localised flow and discontinuous streamlines.

3.4. Correction factors for the cubic law

The fracture permeability obtained from our simulations is 50 to 80 % less than that calculated using the cubic law approximation. Several authors have tried to establish correction factors, accounting for parameters such as surface roughness and tortuosity. Zimmerman & Bodvarsson [3] defined correction factors for the aperture (eq. 2). The roughness correction factor C_r depends on the standard deviation of the aperture. The tortuosity factor C_t depends on the

fracture closure ratio, i.e. the proportion of the fracture plane that is occupied by obstructions. This factor was modified by Walsh et al. [4] due to a percolation threshold at contact ratios of 50 % and above. The general trend is, that the higher the closure ratio, the higher the deviation from the cubic law. The closure ratio required to obtain the same deviation from the cubic law in our simulations and including the correction factor by Zimmerman & Bodvarsson is around 0.2 to 0.3. Looking at the dependence of fracture permeability on mean aperture and standart deviation of the mean aperture, i.e. the spread of the aperture distribution, there is a clear trend that the deviation from the cubic law is decreasing with increasing mean aperture and increasing standart deviation (fig. 6 d,e).

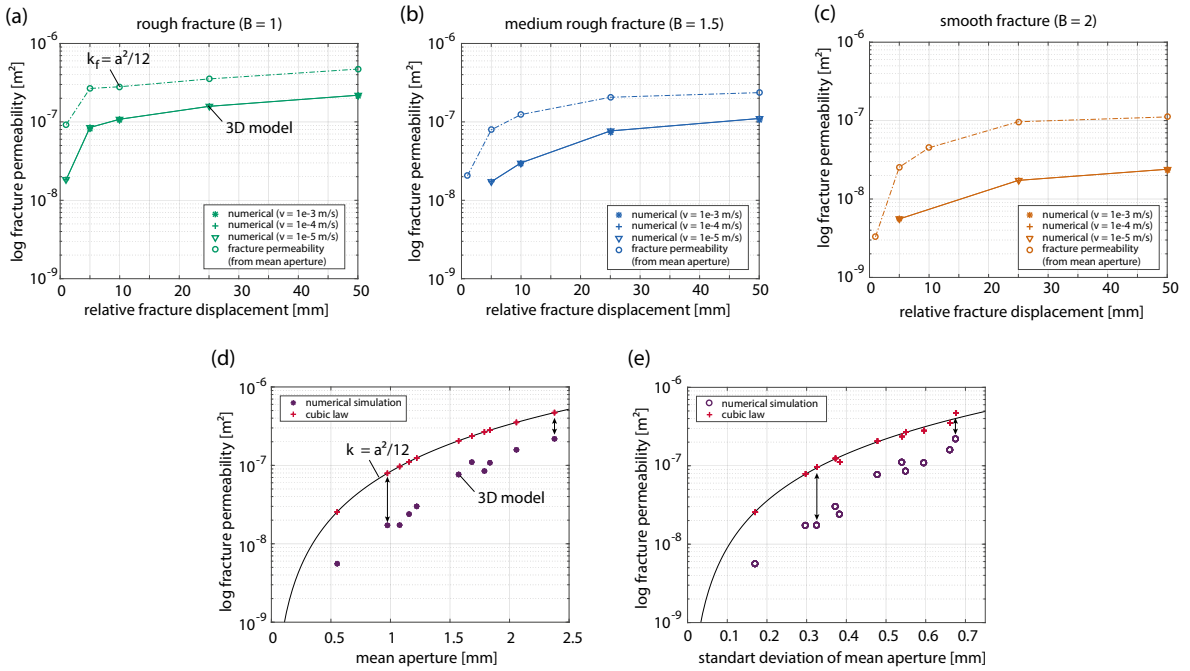

Fig. 6. Fracture permeability depending on relative fracture displacement calculated using the cubic law and the numerically derived permeability for three different levels of roughness: (a) $B = 1$, (b) $B = 1.5$, (c) $B = 2$. (c) Simulated fractured permeability highly depends on the mean aperture. (d) Fracture permeability depending on the mean aperture and (e) standard deviation of mean aperture.

4. Discussion

The mean aperture $\langle a \rangle$ and the aperture distribution for one single fracture is dependent on the fracture offset (fig. 3). Since permeability is a function of the aperture, it is dependent on the fracture offset as well. However, the simulations show that this relation cannot be simply addressed with the Hagen Poiseulle solution of the cubic law [2]. The cubic law assumption of two parallel plates with a constant aperture and laminar flow conditions will be violated in fractures with rough surfaces. Natural fractures with rough surfaces always have a smaller permeability than approximated by the cubic law (fig. 6). Intuitively, the rougher a fracture, the more deviation from the cubic law can be expected. Our simulations show, that rough and displaced fractures have a smaller deviation from the cubic law due to the higher overall aperture which is distributed more equally over the area of the fracture. Similar to the observations by Méheust and Schmittbuhl [7], roughness becomes less meaningful at larger apertures, giving closer results to the cubic law.

Comparing correction factors for the cubic law provided in other studies, for example Zimmerman & Bodvarsson [3] or Jin et al. [5], the calculation of the required parameters from our models remains difficult. The tortuosity factor, i.e. the closure ratio, in Zimmerman & Bodvarsson [3] cannot be calculated correctly. This is because the number of contacting points is very little due to the superposition principle of two fracture surfaces based on the numerical surface heights and the neglected mechanical deformation of the asperities. To obtain the same deviation from the

cubic law as provided by the numerical simulation results, the fracture closure ratio would need to be around 0.2 to 0.3. This means, that for a our fracture models, i.e. a model with the mean aperture of 1.8 mm, all apertures below 1.5 mm must be regarded as closed. It remains difficult to relate this value to a possible closure rate under normal stresses acting perpendicular to the fracture planes in real systems.

Looking at the relation of roughness and displacement, one might argue that the higher the displacement, the higher the permeability. Considering the fact that no mechanical deformation of asperities is involved in our simulations, real fracture asperities will be damaged, due to the normal stress acting perpendicular to a fracture [14, 15, 16]. This will effectively reduce permeability. Asperity deformation in smooth fractures is most likely reduced compared to rough fractures, due to the higher contact area ratio. A balance between displacement and deformation needs to be found for an optimum permeability prediction. Furthermore, no leak-off of fluid from the fracture into the surrounding rock is considered in the models presented in this studies.

5. Conclusions

In this study, 3D numerical flow simulations were performed to investigate the flow behaviour in rough fractures. By use of this approach, correlation between shear displacement and mean aperture, shear displacement and permeability, as well as surface roughness and permeability can be obtained. This hydraulic modeling approach can be applied for artificial as well as real systems. We found in our study, that the mean aperture is increasing with increasing shear displacement when the deformation of the fracture asperities is neglected. Furthermore, the lower the shear displacement, a larger number of small channels with low velocity form. Localizing of flow in smooth and displaced fractures causes a discontinuous flow velocity field. Furthermore, the more smooth a displaced fracture, the higher the deviation from the cubic law. The main controlling parameter on fracture permeability is the mean aperture. Including numerical errors and errors caused by the permeability calculation using mean pressures from the flow simulations, the real fracture permeability is 50 to 80% lower than that calculated using the cubic law approximation. In the future, we aim to include fracture-matrix systems in our simulations to allow for the quantification of the flow volumes in the matrix and the fracture, as well as to quantify the impact of fluid leak-off from the matrix into the host rock.

Acknowledgements

Acknowledgements: This study is performed in the framework of the SURE project. The SURE project has received funding from the European Unions Horizon2020 research and innovation programme under grant agreement No 654662. Thanks to Prof. Dr. Ramon Hanssen (TU Delft) for giving permission to use his fracture generation script.

References

[1] Hofmann, H., Babadagli, T., and Zimmermann, G. (2014). Numerical simulation of complex fracture network development by hydraulic fracturing in naturally fractured ultratight formations. *Journal of Energy Resources Technology*, 136:4 (2014), 042905.

[2] Witherspoon, P. A., Wang, J. S., Iwai, K., and Gale, J. E. (1980). "Validity of cubic law for fluid flow in a deformable rock fracture." *Water resources research*, 16:6 (1980): 1016–1024.

[3] Zimmerman, R. W., and Bodvarsson, G. S. (1996). Hydraulic conductivity of rock fractures. *Transport in porous media*, 23:1 (1996), 1–30.

[4] Walsh, Robert, McDermott, Chris, and Kolditz, Olaf. (2008) "Numerical modeling of stress-permeability coupling in rough fractures." *Hydrogeology Journal* 16 (2008): 613–627.

[5] Jin, Y., Dong, J., Zhang, X., Li, X., and Wu, Y. (2017). Scale and size effects on fluid flow through self-affine rough fractures. *International Journal of Heat and Mass Transfer* 105 (2017): 443–451.

[6] Méheust Y. and Schmittbuhl J. (2001). Geometrical heterogeneities and permeability anisotropy of rough fractures. *Journal of Geophysical Research* 106 (2001): 2089–2102.

[7] Méheust Y. and Schmittbuhl J. (2000). Flow enhancement of a rough fracture. *Geophysical Research Letters* 27 (2000): 2989–2992.

[8] Zhou H.W. and Xie H. (2004). Anisotropic characterization of rock fracture surfaces subjected to profile analysis. *Physics Letters A* 325 (2004): 355–362.

[9] Blöcher, M. G., Zimmermann, G., Moeck, I., Brandt, W., Hassanzadegan, A., and Magri, F. (2010). 3D numerical modeling of hydrothermal processes during the lifetime of a deep geothermal reservoir. *Geofluids*, 10:3 (2010), 406-421.

[10] Zimmermann, G., Moeck, I., and Blcher, G. (2010). Cyclic waterfrac stimulation to develop an enhanced geothermal system (EGS)conceptual design and experimental results. *Geothermics*, 39:1 (2010), 59–69.

[11] Hofmann, H., Blcher, G., Milsch, H., Babadagli, T., and Zimmermann, G. (2016). Transmissivity of aligned and displaced tensile fractures in granitic rocks during cyclic loading. *International Journal of Rock Mechanics and Mining Sciences*, 87 (2016), 69-84.

[12] Milsch, H., Hofmann, H., and Blcher, G. (2016). An experimental and numerical evaluation of continuous fracture permeability measurements during effective pressure cycles. *International Journal of Rock Mechanics and Mining Sciences*, 89 (2016), 109-115.

[13] Cacace, Mauro, and Blöcher, Guido. (2015) "MeshIt - a software for three dimensional volumetric meshing of complex faulted reservoirs." *Environmental Earth Sciences* 74:6 (2015): 5191–5209.

[14] Crawford, B. R. (1998). Experimental fault sealing: shear band permeability dependency on cataclastic fault gouge characteristics. *Geological Society, London, Special Publications*, 127:1 (1998), 27–47.

[15] Watanabe, N., Hirano, N., and Tsuchiya, N. (2009). Diversity of channeling flow in heterogeneous aperture distribution inferred from integrated experimental-numerical analysis on flow through shear fracture in granite. *Journal of Geophysical Research: Solid Earth*, 114:B4 (2009).

[16] Elkhoury, J. E., Niemeijer, A., Brodsky, E. E., and Marone, C. (2011). Laboratory observations of permeability enhancement by fluid pressure oscillation of in situ fractured rock. *Journal of Geophysical Research: Solid Earth*, 116:B2 (2011).